

IMPROVED ADJUSTABLE BOUNDARY CONDITION FOR THE 2-D DIGITAL WAVEGUIDE MESH

Antti Kelloniemi

Telecommunications Software and Multimedia Laboratory
Helsinki University of Technology, Finland
antti.kelloniemi@tkk.fi

ABSTRACT

The digital waveguide (DWG) mesh is a method for simulating wave propagation in multiple dimensions. Boundary conditions are needed for modeling changes in wave propagation media such as walls and furniture in a room or boundaries of a resonating membrane of a musical instrument. The boundary conditions have been solved for a one-dimensional DWG structure, but there is no known exact solution for the multi-dimensional mesh. In this work, a new boundary structure is introduced for modeling reflection coefficient values $-1 \leq r \leq 1$ in two dimensions. The new method gives remarkably more accurate results than the earlier approximations, especially at the low absolute values of r . At incident angles of $\Theta < 60^\circ$, the absolute error of reflection coefficient r is below 0.1 at frequencies $0.004 < f < 0.222$ relative to the sampling frequency and at $60^\circ \leq \Theta \leq 80^\circ$ the same result is reached at $0.005 < f < 0.114$.

1. INTRODUCTION

A variety of methods has been suggested for acoustic modeling. Choice of the preferred method depends on the size of the object, frequency band and amount of detail to be modeled. Unlike geometrical methods such as ray tracing or image source method widely used in room acoustics modeling, the digital waveguide (DWG) mesh first introduced for acoustical instrument modeling inherently includes the diffraction and interference effects into the model [1, 2, 3, 4]. It is a promising method especially for modeling small rooms and low frequencies, where the geometrical methods typically fail.

The DWG structure in its one-dimensional form can be used for modeling the acoustics of, for example, strings and pipes. It is constructed by connecting two parallel delay lines together with scattering junctions at every unit delay location. Changes in wave propagation medium can be modeled using admittance coefficients at the junctions.

Extending the DWG method to two and three dimensions makes it possible to model the acoustics of membranes, resonating bodies of musical instruments or rooms, for example. In multiple dimensions, a mesh is formed by joining more delay lines together. This is accomplished by adding more input and output ports to each scattering junction forming the nodes of the mesh.

The mesh topology can be chosen to be one of the many regular forms. Most common are the triangular and the rectilinear mesh. The rectilinear topology has been used in this work, as the structure made of squares is relatively easy to handle. Numerical dispersion errors appearing in the method are solved using the techniques introduced by Savioja and Välimäki [5]: Interpolation

is described in Section 2 and used throughout the paper, frequency warping was utilized only in Section 4.2.

Boundary conditions are simple to implement in one-dimensional DWG structure, as they can be obtained straight from the delay line updating functions. In multiple dimensions the case is more complicated. The only boundary condition that is common for all dimensionalities is the phase inverting perfect reflection that is obtained when the junction values at the edges of the mesh are bound to zero. Other reflection coefficient values are traditionally implemented by use of one-dimensional boundary conditions, irrespective of the model dimensionality. This approach gives good results with high reflection coefficient values, but fails with absorbing boundaries [4, 6].

As shown by Murphy and Mullen [7], the absorbing boundary condition with reflection coefficient value $r = 0$ could be implemented in multi-dimensional mesh structures by use of the Taylor series approximation. The result was better than the one obtained with the use of the basic 1-D solution, but as the method was still one-dimensional, direction dependent errors remained and reflection magnitude was below -25 dB only when the incident angle was below 68° relative to the normal incidence. The first two-dimensional solution for $r = 0$, namely the spatial filter-based absorbing boundary condition, was introduced in 2005 by Kelloniemi et al. [8]. With use of this solution, the reflection magnitude was radically diminished and was below -25 dB at angles of incidence up to 79° .

Recently, a new solution for modeling the reflection coefficient values $r = 0 \dots 1$ in two dimensions was introduced [6]. While this solution performs better than the basic 1-D method when low reflection coefficient values are needed, it has evident problems at the low frequencies and can not be used for phase inverting boundary conditions as discussed in Section 3.1.

The new adjustable boundary condition introduced in Section 3.2. solves both of these problems. It relies on the use of the admittance coefficients at the junctions for modeling the boundary and the spatial filter-based absorbing boundary condition for truncating the mesh. The basic 1-D adjustable boundary condition was chosen as a reference when the new boundary condition was tested as described in Section 4, as it is the only earlier solution known to be stable with the full range of reflection coefficient values from $r = -1$ to $r = 1$.

As the 2-D and 3-D mesh structures have much in common, the boundary conditions are here implemented only for the 2-D case and extending them to 3-D has been left for future work.

2. INTERPOLATED 2-D DIGITAL WAVEGUIDE MESH

The digital waveguide (DWG) mesh is a computational structure for approximating multidimensional wave propagation. The mesh is constructed of scattering junctions positioned at the regular node locations and interconnected with bidirectional signal lines.

The updating function has two equivalent formulations. The digital waveguide formulation uses traveling wave variables representing the wave decomposition of the signal propagating in the mesh. Instead in the finite-difference time-domain formulation, physical Kirchhoff variables are used.

Because the practice of using mesh-related concepts in the literature is somewhat inconsistent, we want to be more specific here. We use the term W-mesh for the wave variable formulation with delays between junctions and K-mesh for the structure based on the Kirchhoff variable formulation with state variables within nodes. The two forms have been shown to be functionally equivalent, but based on W- and K-variables, respectively [9]. In W-mesh, values traveling between nodes are saved, so two memory units are needed per each interconnection. Instead in K-mesh only two values per node are saved [4]. Knowing the traveling wave component values is useful for some applications, but in this paper we apply particularly the K-mesh formulation due to its computational efficiency and reduced memory requirements.

Van Duyne and Smith derived the equations for the lossless interconnection of several one-dimensional delay lines [2]. The difference equation for the scattering junctions of an N -dimensional rectilinear K-mesh was derived in their results as

$$p_c(n) = \frac{\sum_{l=1}^{2N} Y_l p_l(n-1)}{\frac{1}{2} \sum_{l=1}^{2N} Y_l} - p_c(n-2), \quad (1)$$

where Y is the admittance of an interconnection, p represents the signal value at a junction at time step n , subscript c denotes the junction to be calculated and index l denotes its $2N$ axial neighbors. The maximum simulation frequency f is restricted to a quarter of the sampling frequency f_s of the mesh.

For minimizing the direction dependent dispersion error appearing in the rectilinear mesh topology, each junction has to be connected also with its diagonal neighbors [5]. The resulting difference equation for the nodes of a two-dimensional interpolated rectangular mesh is

$$p_c(n) = \frac{\sum_{l=1}^3 \sum_{k=1}^3 Y_{l,k} h_{l,k} p_{l,k}(n-1)}{\frac{1}{2} \sum_{l=1}^3 \sum_{k=1}^3 Y_{l,k} h_{l,k}} - p_c(n-2), \quad (2)$$

where $h_{l,k}$ are interpolated weighting coefficients for each node. Coefficient values $h_d = 0.375930$ for diagonal connections and $h_c = 1.50372$ for the center node connection are used in signal value interpolation between the diagonal nodes and the center node for making the wave propagation speed apparently same as in the axial connections weighted with $h_a = 1.24814$ [5]. With the admittance values they form a convolution kernel

$$h = \begin{bmatrix} Y_{1,1}h_d & Y_{2,1}h_a & Y_{3,1}h_d \\ Y_{1,2}h_a & Y_{2,2}h_c & Y_{3,2}h_a \\ Y_{1,3}h_d & Y_{2,3}h_a & Y_{3,3}h_d \end{bmatrix} \quad (3)$$

applied to the junction p_c and its immediate neighbors.

When all port admittances of a certain junction are equal, (2) reduces to

$$p_c(n) = \frac{1}{4} \sum_{l=1}^3 \sum_{k=1}^3 h_{l,k} p_{l,k}(n-1) - p_c(n-2). \quad (4)$$

3. ADJUSTABLE BOUNDARY CONDITIONS

For the simulation of real or virtual acoustic spaces, an implementation of controllable boundary conditions is needed. In an optimal case, the reflection coefficient value of the wall or other boundary structure would be known at multiple frequencies and angles of incidence, and a model could be adjusted to these values. At the current state we are lacking both the extensive measurement data of real boundaries and a method for modeling them in a digital waveguide mesh. As a step towards the goal, a method is derived where the reflection coefficient can be set to a constant real value r for all frequencies and incident angles. As the material parameters are often given as constants in octave bands, the simulation could be run separately for each of them.

3.1. Previous methods

The discrete boundary condition of the acoustical pressure is traditionally constructed in the digital waveguide mesh by adding special boundary nodes outside the mesh edges and interconnecting each of them only with one neighboring node at the edge of the mesh. Irrespective of the model dimensionality, the boundary node values are calculated as in one dimension:

$$p_B(n) = (1+r)p_1(n-1) - rp_B(n-2), \quad (5)$$

where subscript B denotes the boundary node and subscript 1 represents its perpendicular neighbor [4]. The two terms on the right hand side of (5) represent the sound pressure in front of the boundary one time step ago and the sound pressure reflected from the boundary two time steps ago, respectively.

In earlier work it has been noted that in a multi-dimensional mesh this basic solution gives good results only with high reflection coefficient values. Unwanted reflection occurs with the low values of r due to the change in dimensionality at the boundary [4, 6]. The absorbing boundary condition was then improved by extending it to a Taylor series [7]. With use of the first order solution of the series, a method for adjustable boundary condition performing better at the low reflection coefficient values was introduced [6]. The boundary node value was now calculated as

$$p_B(n) = 2p_1(n-1) - (1-r)p_2(n-2) - rp_B(n-2). \quad (6)$$

Unfortunately the suggested method did not offer a general solution. It was restricted only for phase preserving reflections where $r \geq 0$ and significant errors occurred at the low frequencies relative to the sampling frequency. The low frequency performance was improved by use of a second-order FIR filter, but that led to making the simulation in even narrower frequency bands. For these reasons demand for a better solution remained.

3.2. New method

It has been known from the beginning of the research with the digital waveguide mesh that changes in the wave propagation media can be modeled using the admittance constants at the scattering junctions as shown in (1) [2].

As a new boundary solution, the change in admittance is modeled at nodes on a line called *the admittance boundary*. The width of the *boundary layer* between the admittance boundary and the mesh edge is marked with W in Fig. 1(a) describing the structure.

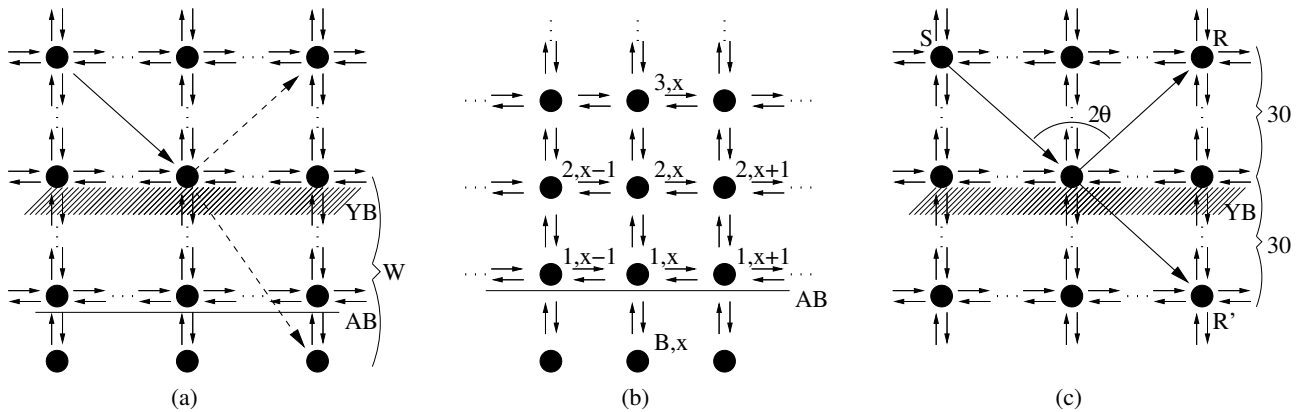


Figure 1: The admittance boundary structure, absorbing boundary condition nodes and the test setup. For simplicity the diagonal connections have been omitted. (a) shows the new boundary structure: the shaded area represents the admittance boundary (YB) located W nodes away from the absorbing boundary (AB), which is at the mesh edge marked with the solid line. Solid arrow represents the signal arriving to the admittance boundary and dashed lines show the reflected and absorbed signal parts. (b) shows the nodes involved in (9). As indicated in (c), the test setup consisted of the source (S) and the receiver (R) placed in line 30 nodes apart from the admittance boundary. The freefield signal used as a reference was received at a mirror image location (R').

At a junction on the admittance boundary, the admittance values of the connections pointing towards the mesh edge are set to

$$Y = \frac{1-r}{1+r}, \quad (7)$$

where r is the desired reflection coefficient [10]. At the limit, where $r = -1$, Y goes to infinity. In this case a large constant value is used instead.

The admittance value at the center node is used for interpolation with the diagonal nodes. It is set to the average of the admittances at the diagonal connections. For example, if the boundary is at the direction where index $k = 3$, the kernel at the admittance boundary is

$$h = \begin{bmatrix} h_d & h_a & h_d \\ h_a & \frac{2Y+2}{4}h_c & h_a \\ Yh_d & Yh_a & Yh_d \end{bmatrix}. \quad (8)$$

Equally in case of a rectilinear 2-D corner, admittance values of two axial and three diagonal connections would be set to Y and the center node value would be weighted accordingly.

Depending on the admittance coefficient, part of the signal gets reflected and part passed through the admittance boundary as indicated with dashed arrows in Fig. 1(a). The signal propagated to the mesh edge is absorbed using the spatial filter-based absorbing boundary condition [8]. The absorbing boundary node value is calculated as

$$\begin{aligned} p_B(n) = & h_{Ba1}p_{1,x}(n-1) \\ & + \frac{h_{Bd1}}{2}[p_{1,x-1}(n-1) + p_{1,x+1}(n-1)] \\ & + h_{Ba2}p_{2,x}(n-2) \\ & + \frac{h_{Bd2}}{2}[p_{2,x-1}(n-2) + p_{2,x+1}(n-2)] \\ & + h_{Ba3}p_{3,x}(n-3), \end{aligned} \quad (9)$$

where the subscripts of p designate the node coordinates as indicated in Fig. 1(b) and the axial and diagonal filter coefficients have values $h_{Ba1} = 2.42087845$, $h_{Ba2} = -2.33808068$, $h_{Ba3} = 0.90809890$, $h_{Bd1} = 0.48591057$, and $h_{Bd2} = -0.47683624$ [8]. As also the diagonal neighbors are used in calculation of the value p_B , this boundary condition can not be used at the corners of the mesh, where the boundary node values are therefore calculated with (5) having $r = 0$.

As the coefficients in (9) are optimized for homogenous mesh, the boundary layer width has to be at least $W = 4$ so that the admittance boundary is out of the reach of the boundary node update equation. The boundary layer can anyway be made as wide as one wishes and even multiple admittance boundaries can be implemented one after another to model layered boundary structures.

4. COMPARISON SETUP AND RESULTS

The performances of the old and the new boundary structures were tested with simulations. First the magnitude responses of the boundaries were resolved at multiple frequencies and incident angles. In the second simulation, effects of the new boundary structure to the mode frequencies of a rectangular 2-D mesh was tested by implementing the admittance boundary on all edges of the mesh.

4.1. Reflection magnitude

The simulations for resolving the magnitude of the signal reflected from the admittance boundary were executed in a 2-D mesh of $1000 \times (300 + W)$ junctions, where W is the boundary layer width shown in Fig. 1(a). A unit impulse was used as an input signal at location $(300, 30 + W)$. Receivers were located at each node on a line located at the equal distance from the boundary with the source as shown in Fig. 1(c). The simulation was run for 700 time steps. The signal component that passed directly from the source to the receiver was subtracted from the data. The right half

of the Hanning window function was used for windowing the last half of the received signal to avoid the truncation error in calculation of the spectra. For resolving the achieved reflection coefficient value, the resulting signal level was compared to the level of a signal representing the ideal perfect reflection. This reference signal was received at a mirror image location shown in Fig. 1(c) on the other side of the admittance boundary when the boundary was non-reflective ($Y = 1$) and the mesh edges were far enough for not causing any reflections. The absolute error of the achieved reflection magnitude was defined by subtracting the set value of r from the received frequency responses. Relative error value was calculated by dividing the absolute value with r . Maximum error values were calculated for the basic 1-D solution (5) and for the new admittance boundary solution with boundary layer widths $W = 4$ and $W = 40$. The results are shown for three ranges of incident angle values, namely $0^\circ \leq \Theta < 30^\circ$, $30^\circ \leq \Theta < 60^\circ$, and $60 \leq \Theta \leq 80^\circ$ relative to the normal incidence, having 35, 69 and 202 regularly spaced receiving points respectively. Receiving points at the incident angles beyond 80° would require very large mesh sizes, so those were omitted. The maximum error was found from all received magnitude responses individually for each frequency value. The simulation was repeated for 101 values of reflection coefficient at $r = -1 \dots 1$.

The results are plotted in Figures 2, 3 and 4. Contour lines are drawn on the surface plots at absolute error value 0.1 and relative error value 10%. The error plots in Fig. 2 show that at angles of incidence $\Theta < 30^\circ$ the basic solution could be used when negative reflection coefficient values are needed. At the positive values of r more important in room acoustics modeling, the error grows remarkably with coefficient values $r < 0.6$. By contrast, the new solution has absolute error values below 0.1 with all values of r at relative frequencies $0.004 < f < 0.222$. On the next range of incident angles $30^\circ \leq \Theta < 60^\circ$ in Fig. 3, the basic solution could be useful only with absolute values of the reflection coefficient $|r| > 0.5$, because below that the accurate frequency band gets narrow. The new admittance boundary solution can still be used on same frequency range as in the previous incident angle range, with all values of r .

The error at high relative frequencies grows at the high angles of incidence, as seen in Fig. 4 where the maximum error at angles $60^\circ \leq \Theta \leq 80^\circ$ is illustrated. Still there is a frequency band $0.005 < f < 0.114$, where the new method has absolute error value below 0.1 at all values of r , contrary to the basic method that could be used only at the highest and lowest reflection coefficient values at about $r > 0.6$ or $r < -0.8$. The minor error values of the new method at $r \approx 0$ are especially notable.

The small reflections occurring from the absorbing boundary cause the comb filter effect seen as stripes in the frequency responses of the lowermost images in Figures 2, 3 and 4, where $W = 40$. Increasing the boundary layer width is seen beneficial only at the very smallest absolute values of the reflection coefficient, where insignificantly smaller relative error values are obtained.

4.2. Mode frequencies

Besides the reflection magnitude, the delay caused at the boundary is an important factor in simulations, as it affects the mode frequencies of the model. For testing the effect the admittance boundary has to the mode frequencies, a 2-D mesh with 18×18 junctions was built including the boundary layers of 4 nodes on

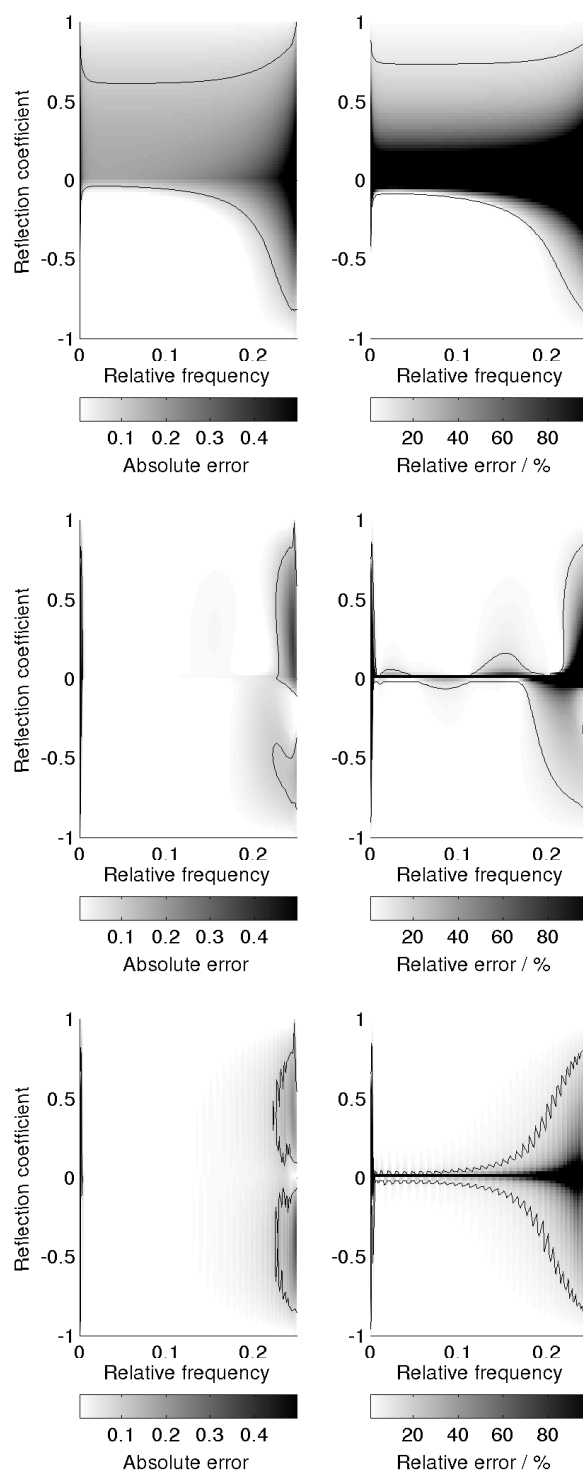


Figure 2: Maximum absolute and relative error of the received reflection coefficient in the original adjustable boundary condition (5) (top) and in the new adjustable boundary condition with $W = 4$ (middle) and $W = 40$ (bottom) at incident angles $0^\circ \leq \Theta < 30^\circ$. Contour lines are drawn at absolute error value 0.1 and relative error value 10%.

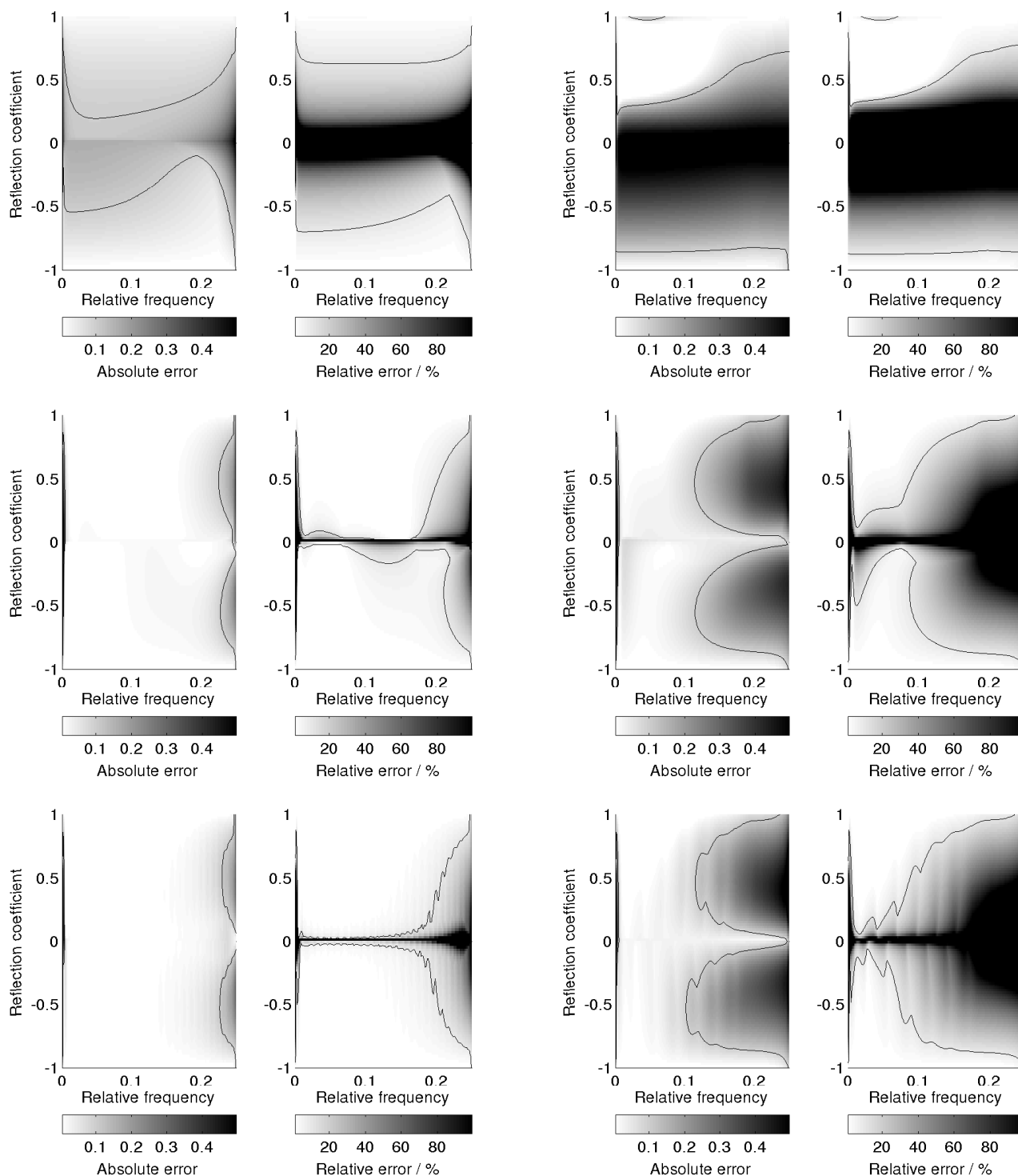


Figure 3: Maximum error of the received reflection coefficient in the original adjustable boundary condition (5) (top) and in the new adjustable boundary condition with $W = 4$ (middle) and $W = 40$ (bottom) at incident angles $30^\circ \leq \Theta < 60^\circ$. Contour lines are drawn as in Fig. 2.

Figure 4: Maximum error of the received reflection coefficient in the original adjustable boundary condition (5) (top) and in the new adjustable boundary condition with $W = 4$ (middle) and $W = 40$ (bottom) at incident angles $60 \leq \Theta \leq 80^\circ$. Contour lines are drawn as in Fig. 2.

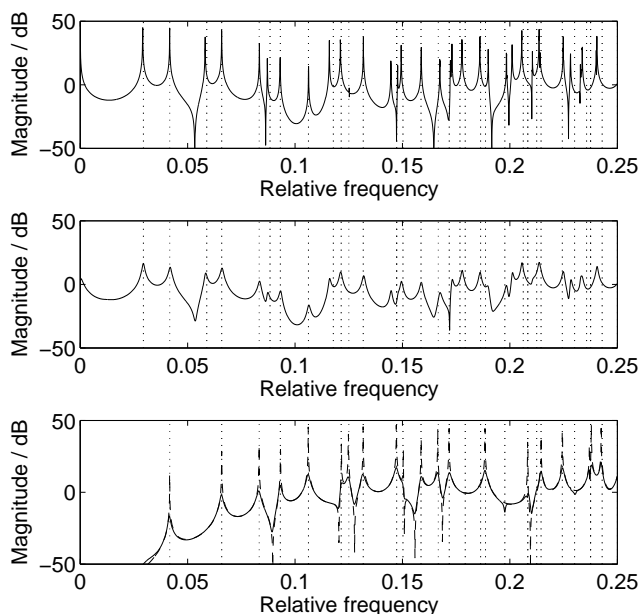


Figure 5: The mode structure of a 2-D mesh with reflection coefficient values $r = 1$ (top), $r = 0.95$ (middle) and $r = -0.95$ (bottom) plotted with solid line. The dotted lines show the theoretical mode locations and the dashed line in the lowermost image is for the ideal solution of $r = -1$.

each edge. Spatial filter-based absorbing boundaries and admittance boundaries were set on all edges of the mesh. Input and output points were located to the corners inside the boundaries at (6, 6) and (12, 12). Unit impulse was used as test signal. The simulation was run for 2^{14} time steps. For reference, theoretical mode locations were calculated [10]. Also the result with reflection coefficient value set exactly to $r = -1$ was computed by binding the admittance boundary junctions to zero. After computing the magnitude spectra, frequency warping [5] was used for minimizing the frequency dependent dispersion error.

The magnitude responses received with reflection coefficient values $r = 1$, $r = 0.95$ and $r = -0.95$ are plotted in Fig. 5. The mode frequencies match fairly well with the theoretical values. The error of the mode locations grows with the frequency but is equal for all values of r . Some modes are missing because the input and output points were located one node location away from the mesh edges. This was done because for the ideal solution for $r = -1$ the boundary junctions were bound to zero. The ideal response is drawn with dashed line in the lowermost plot. It should be noted that its mode frequencies match perfectly with those of the admittance boundary. Therefore it can be stated, that the differences in mode frequencies compared to the theoretical values are not due the new boundary condition, but are caused by the mesh structure.

5. CONCLUSIONS

A new adjustable boundary condition for the digital waveguide mesh was introduced for modeling the changes in wave propagation media. The boundary structure consists of the admittance

boundary, behind which a spatial filter-based absorbing boundary is constructed for truncating the mesh. The method was tested in a two-dimensional K-mesh. Significantly better results were obtained than with the basic one-dimensional boundary condition. It was noted that the results were not significantly improved by extending the boundary layer width between the admittance boundary and the edge of the mesh. As a continuation of the research, the method will be extended to three dimensions. Also the possibility to implement frequency dependent boundary conditions using layered admittance boundary structures will be investigated.

6. ACKNOWLEDGEMENTS

The author has received funding from the Academy of Finland (project no. 201050) and the Nokia Foundation. He would like to thank professors Vesa Välimäki, Lauri Savioja and Matti Karjalainen for their helpful suggestions.

7. REFERENCES

- [1] J. O. Smith, *Music Applications of Digital Waveguides*, Tech. Rep. STAN-M-39. CCRMA, Stanford University, CA, May 1987.
- [2] S. Van Duyne and J. O. Smith, "Physical modeling with the 2-D digital waveguide mesh," in *Proc. Int. Computer Music Conf. (ICMC)*, Tokyo, Japan, September 1993, pp. 40–47.
- [3] S. Van Duyne and J. O. Smith, "The 2-D digital waveguide mesh," in *Proc. IEEE Workshop on Applications of Signal Processing to Audio and Acoustics (WASPAA'93)*, New Paltz, NY, October 1993.
- [4] L. Savioja, T. Rinne, and T. Takala, "Simulation of room acoustics with a 3-D finite difference mesh," in *Proc. Int. Computer Music Conf. (ICMC)*, Aarhus, Denmark, September 1994, pp. 463–466.
- [5] L. Savioja and V. Välimäki, "Reducing the dispersion error in the digital waveguide mesh using interpolation and frequency warping techniques," *IEEE Trans. Speech and Audio Processing*, vol. 8, pp. 184 – 194, March 2000.
- [6] A. Kelloniemi, D. T. Murphy, L. Savioja, and V. Välimäki, "Boundary conditions in a multi-dimensional digital waveguide mesh," in *Proc. IEEE Int. Conf. Acoust. Speech Signal Processing (ICASSP)*, Montreal, Canada, May 2004, vol. 4, pp. 25 – 28.
- [7] D. T. Murphy and J. Mullen, "Digital waveguide mesh modelling of room acoustics: improved anechoic boundaries," in *Proc. Int. Conf. Digital Audio Effects (DAFx)*, Hamburg, Germany, September 2002, pp. 163 – 168.
- [8] A. Kelloniemi, L. Savioja, and V. Välimäki, "Spatial filter-based absorbing boundary for the 2-D digital waveguide mesh," *IEEE Signal processing letters*, vol. 12, no. 2, pp. 126–129, February 2005.
- [9] M. Karjalainen and C. Erku, "Digital waveguides vs. finite difference schemes: Equivalence and mixed modeling," *EURASIP J. Applied Signal Process.*, vol. 2004, no. 7, pp. 978–989, June 2004.
- [10] H. Kuttruff, *Room acoustics*, Spon Press, London, 4th edition, 2000.